Quantitative probing of tip-induced local cooling with a resistive nanoheater/thermometer

Sina Hamian, Jeonghoon Yun, Inkyu Park, and Keunhan Park

Citation: Appl. Phys. Lett. **109**, 253114 (2016); doi: 10.1063/1.4972792
View online: http://dx.doi.org/10.1063/1.4972792
View Table of Contents: http://aip.scitation.org/toc/apl/109/25
Published by the American Institute of Physics

Quantitative probing of tip-induced local cooling with a resistive nanoheater/thermometer

Sina Hamian,[1] Jeonghoon Yun,[2] Inkyu Park,[2] and Keunhan Park[1,a)]
[1]*Department of Mechanical Engineering, University of Utah, Salt Lake City, Utah 84112, USA*
[2]*Department of Mechanical Engineering, Korea Advanced Institute of Science and Technology (KAIST), Daejeon 305-701, South Korea*

(Received 23 September 2016; accepted 8 December 2016; published online 23 December 2016)

This article reports the investigation of tip-induced local cooling when an atomic force microscope (AFM) cantilever tip scans over a joule-heated Pt nanowire. We fabricated four-point-probe Pt resistive nanothermometers having a sensing area of 250 nm × 350 nm by combining electron-beam lithography and photolithography. The electrical resistance of a fabricated nanothermometer is ~27.8 Ω at room temperature and is linearly proportional to the temperature increase up to 350 K. The equivalent temperature coefficient of resistance is estimated to be $(7.0\pm0.1)\times10^{-4}\,\mathrm{K}^{-1}$. We also joule-heated a nanothermometer to increase its sensing area temperature up to 338.5 ± 0.2 K, demonstrating that the same device can be used as a nanoheater. An AFM probe tip scanning over a heated nanoheater/thermometer's sensing area induces local cooling due to heat conduction through solid-solid contact, water meniscus, and surrounding air. The effective contact thermal conductance is 32.5 ± 0.8 nW/K. These results contribute to the better understanding of tip-substrate thermal interactions, which is the fundamental subject in tip-based thermal engineering applications. *Published by AIP Publishing.*
[http://dx.doi.org/10.1063/1.4972792]

Over the past two decades, tip-based thermal engineering has made significant advances to enable various cutting-edge nanoscale applications, such as scanning thermal microscopy (SThM) for nanoscale thermal imaging[1–4] and analysis,[5–8] thermally-based topographic imaging,[9–11] mid-infrared nanospectroscopy,[12–14] high-density data storage,[15–18] and nanomanufacturing.[19–26] These applications have created strong demands to study the fundamentals of local thermal transport due to a tip contact. Advancements in nanothermometry have allowed the experimental studies of tip-substrate thermal transport mechanisms and local temperature distributions.[27–31] Nanothermometry techniques developed to date include near-field optical thermometry,[32] tip-enhanced Raman thermometry,[33–35] tip-based fluorescence microscopy,[36] SThM-based nanothermometry using thermocouple[4,29,37–39] or resistive[31,40,41] probes, and on-substrate thermocouple[42–44] or resistive[28,45] nanothermometry. Among different techniques, four-point-probe resistive thermometry has several advantages over other methods, such as relatively easy fabrication and instrumentation, high precision temperature measurement,[46,47] and the use of the same device as a local heater for thermophysical property measurement.[48–50] However, a relatively large sensing area is required to achieve a high temperature sensitivity for resistive thermometry. On-substrate resistive nanothermometers developed to date have nanoscale confinement in only one direction,[28,45] which has prevented the probing of local thermal transport with a fully nanoscale spatial resolution.

In this article, we present the design, fabrication, and characterization of on-substrate platinum (Pt) resistive nanothermometers having a 250 nm × 350 nm sensing area and its use for quantitative probing of tip-substrate thermal transport. The developed nanothermometers show a linear proportionality of the electrical resistance with increasing temperature, which is a desired performance for reliable temperature measurement. In addition, we demonstrate that the device can be used as a nanoheater by increasing the input current. The resistive nanothermomer/heater is used for the experimental study of tip-induced local cooling in an atomic force microscope (AFM) platform. When an AFM microcantilever probe scans over a heated nanothermometer (or nanoheater) in contact mode, a relatively cold tip induces local cooling from a heated area. Measuring the temperature and heating power changes of the nanothermometer allows the probing of the tip-induced local cooling, from which the effective contact thermal conductance is determined.

Fig. 1(a) shows the schematics and scanning electron microscope (SEM) micrographs of a fabricated four-point resistive nanothermometer device. The detailed fabrication steps of the nanothermometer are provided in Fig. S1 of the supplementary material. The key of the fabrication process is to combine e-beam nanolithography and photolithography techniques to align nanopatterned Pt strips with micropatterned gold (Au) electrical leads. The Au micropatterns cover the Pt nanopatterns with an average area of 3 μm × 3 μm to minimize contact electrical resistance. Pt nanowires and Au electrical leads are 40 nm and 180 nm thick, respectively, according to the AFM measurement shown in Fig. S2. Eight nanothermometers are fabricated on a 1 cm × 1 cm SiNx-on-Si chip. Adjacent nanothermometers are separated by 300 μm for thermal isolation during independent measurements and to provide a suitable platform for the differential measurement scheme. The resistive sensing area

a)Author to whom correspondence should be addressed. Electronic mail: kpark@mech.utah.edu

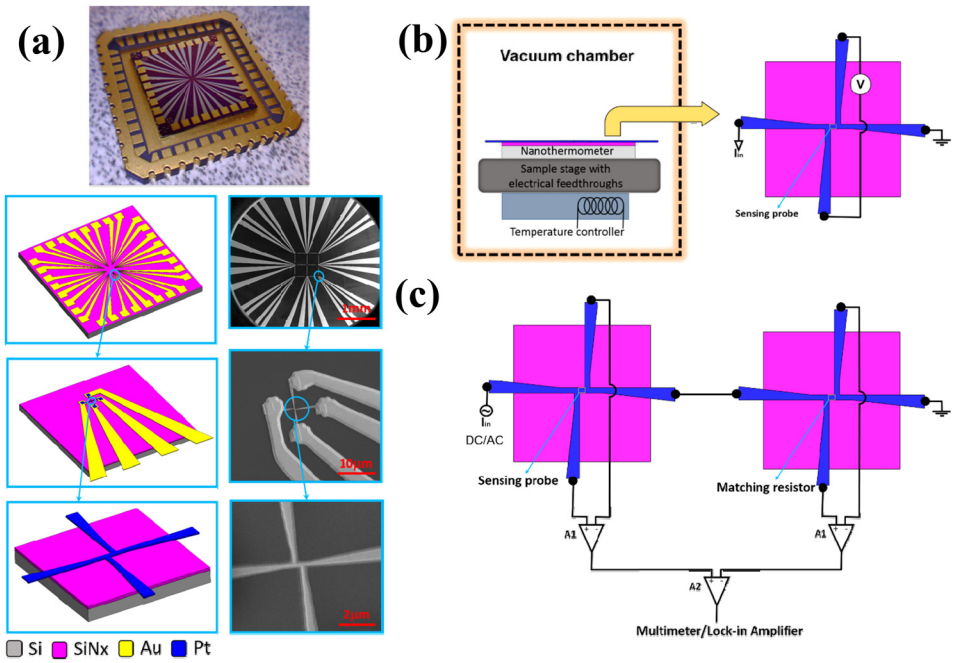

FIG. 1. (a) Picture, schematic, and SEM images of a fabricated chip having eight independent nanothermometer/heaters. (b) Experimental setup for TCR measurement and (c) the differential scheme to isolate the signal of interest to precisely measure relative temperature change of the device.

is at the very center of the Pt nanowires with an area of approximately 250 nm × 350 nm, where 250 nm is the width of the Pt nanopattern and 350 nm is the length of the thermometer sensing area as measured between the centers of the inner electrodes.

The nanothermometers were calibrated in a vacuum chamber equipped with a heater stage and electrical feedthroughs. The heater and a K-type thermocouple in the sample stage are connected to a temperature controller (Cryo-Con 22C) to feedback control the stage temperature with 50 mK accuracy. Fig. 1(b) illustrates the experimental setup for nanothermometer calibration, where the voltage drop across the inner electrodes is measured while a constant input current of 100 μA is applied through the outer electrodes of the nanothermometer. The input current of 100 μA was carefully chosen to guarantee a stable thermometer signal without self-heating the thermometer in a vacuum condition at $\sim 1 \times 10^{-5}$ Torr. The finite element analysis (COMSOL Multiphysics) predicts the temperature increase of the sensing area to be 45 mK when the input current is 100 μA (or the power dissipation of 27.8 μW) in vacuum. A compelling advantage of having multiple thermometers in one chip is to implement a differential scheme for precision measurement. Fig. 1(c) illustrates the differential scheme, where a reference nanothermometer is connected in series with the sensing nanothermometer. Each thermometer is connected to an instrument amplifier (Analog Devices, AD524) with the gain of ×10, and their output signals are supplied to the third instrument amplifier with the gain of ×10 to yield an amplified differential signal (×100) due to a small temperature change of the sensing nanothermometer. The temperature resolution of the nanothermometer under the differential scheme can be determined by conducting a noise spectrum analysis within a small frequency range close to 0 Hz.[46] The power spectral density of the nanothermometer is shown in Fig. S3 in the supplementary material for the frequency range between 0 and 0.5 Hz, from which the noise equivalent voltage is estimated to be 12.96 μV. The corresponding noise equivalent temperature is 410 mK: see the supplementary material for more details.

The base electrical resistance of the nanothermometer used for calibration is $R_0 = 27.82 \pm 0.01\Omega$ at room temperature, which is equivalent to the resistivity of $(7.9 \pm 1.1) \times 10^{-7}$ Ω-m from the geometry of the sensing area (40 nm in thickness, 350 nm in length between two inner electrodes, and 250 nm in width, with approximately 10% uncertainties). It should be noted that the estimated resistivity is almost eight times larger than that of bulk Pt (i.e., 1.06×10^{-7} Ω-m). This high resistivity may be due to the boundary scattering of electrons and defects formed during fabrication.[51] Fig. 2(a) shows the calibration result of a nanothermometer over the temperature range from room temperature to 350 K, where the electrical resistance of the thermometer sensing area is linearly proportional to the temperature increase. The corresponding temperature coefficient of resistance (TCR) is $(7.0 \pm 0.1) \times 10^{-4}\,\mathrm{K}^{-1}$, which is in good agreement with the previous research.[28] From the determined TCR, we can measure the temperature change of the nanothermometer's sensing probe using $\Delta T_S = \Delta V_S/(\alpha \cdot G \cdot I \cdot R_0)$, where ΔV_S and G are the voltage change and the gain of the differential measurement circuit, respectively, α is the TCR, and I is the input current to the nanothermometer.[4,27] We also tested the feasibility of using the nanothermometer device as a heater by increasing the input current in the air. Fig. 2(b) shows the parabolic increases of the thermometer resistance and the power dissipation of the entire Pt nano-strip with the input current increase, demonstrating that the nanothermometer is joule-heated. At the input current of 1.6 mA, the sensing probe temperature becomes 338.5 ± 0.2 K, which is high enough to conduct tip-induced local cooling measurements. It should be noted that further heating was possible but the experiment was stopped at 1.6 mA to avoid thermal damage of the device.

The tip-induced cooling experiment was conducted by raster-scanning the sensing area of a heated nanothermometer

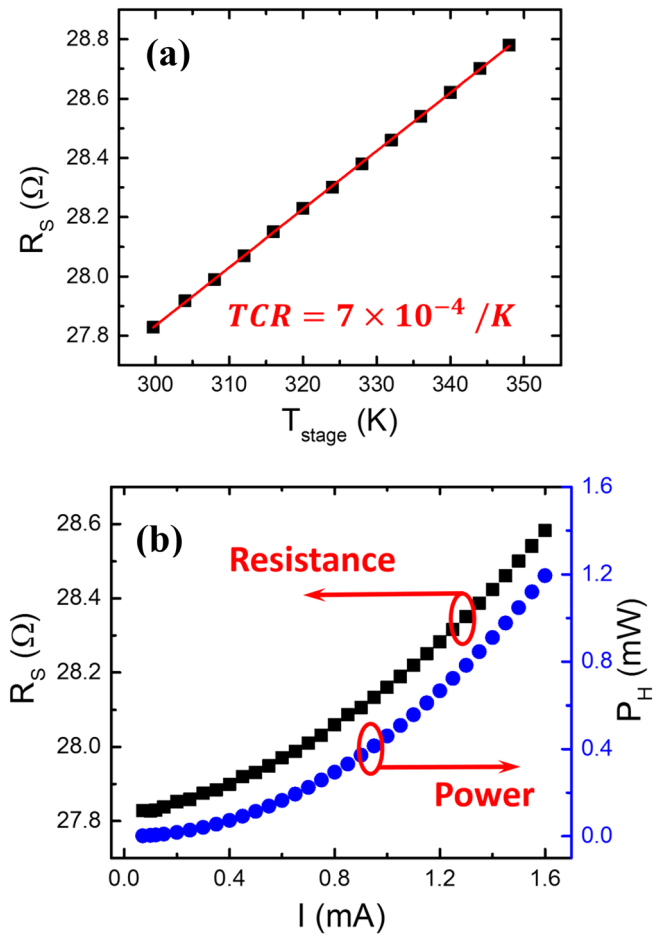

FIG. 2. (a) The electrical resistance of the nanothermometer sensing area as a function of the stage temperature. From the linear proportionality, the TCR of the nanothermometer is determined to be 7.0×10^{-4} K^{-1}. (b) The parabolic curves of the thermometer resistance and power dissipation of the Pt nano-strip demonstrate the heating capability of the device up to 338.5 K.

(or nanoheater) with a silicon AFM cantilever probe (Bruker, FMV-A) and simultaneously mapping topographic and thermometer signals. The tip-induced cooling rate can be determined by $P_C = I\Delta V_H$, where ΔV_H is the voltage change of the entire Pt heater between the outer electrodes, under the assumption that any change in the power dissipation across the Pt heater is due to heat loss to the tip. Fig. 3(a) shows the SEM image of the cantilever probe used for the experiment, which has a pyramidal tip with a 16 μm tip height and 8 nm tip radius. The nanothermometer was joule-heated with the input current of 1.6 mA, raising the temperature of the thermometer sensing area at 338.5 ± 0.2 K. The cantilever scans around the thermometer sensing area ($2\,\mu m \times 2\,\mu m$) in contact mode with the set-point contact force of 15 ± 5 nN. The scanning speed was set to 0.3 μm/s to provide sufficient time for the thermometer to thermally respond to the tip movement, as will be discussed in Fig. 3(c).

Fig. 3(a) shows the topographic image around the thermometer sensing area along with the corresponding temperature and power dissipation images measured by the thermometer. The dark region in the temperature image attests local cooling by the tip when it scans over the heated thermometer sensing area. The tip-induced cooling is better depicted by the average temperature of the nanothermometer sensing area (T_S), power dissipation of the nanoheater (P_H), and the corresponding tip-substrate thermal conductance (G_C) with respect to the tip position in Fig. 3(b). The local tip-substrate thermal conductance is estimated from $G_C = (P_{H,0} - P_H)/(T_S - T_\infty)$, where $P_{H,0}$ is the initial thermometer power dissipation, under the assumption that the tip base temperature remains constant at room temperature T_∞. As the tip scans along the yellow-dashed line in Fig. 3(a), the thermometer sensing area, initially at $T_{S,0} = 338.5 \pm 0.2$ K by $I = 1.6$ mA (or $P_H = 1.19$ mW), cools down due to heat conduction from the heated thermometer to the tip through solid-solid contact, water meniscus, and surrounding air molecules. The gradual change of the thermometer temperature signal follows the same trend as the numerically calculated local temperature distribution across the thermometer as shown in Fig. S4, indicating that the nanothermometer captures the local cooling at different tip positions: maximal cooling at the center due to the highest local temperature. The shoulders at the thermometer edges in Fig. 3(b) are due to sudden changes in contact area between the tip and the thermometer when the tip moves from the thermometer edge to the substrate.[4] We also believe that the slightly asymmetric temperature profile is due to the uneven pyramidal tip shown in Fig. 3(a), which may be convoluted with the thermometer signal.

From Fig. 3(b), the temperature dip depth is $\Delta T_S = 10.1 \pm 0.2$ K when the tip is placed in the center of the thermometer sensing area. The corresponding heat loss is measured to be $\Delta P_H = 923 \pm 15$ nW. The effective contact thermal conductance can be estimated from $\Delta G_C = \Delta P_H/(T_{S,\min} - T_\infty)$, where $T_{S,min}$ denotes the dip temperature of the thermometer sensing area in Fig. 3(b). The estimated thermal conductance is $\Delta G_C = 32.5 \pm 0.8$ nW/K. The equivalent contact thermal resistance is estimated to be $\sim 6.2 \times 10^{-9}$ m^2 K/W by assuming the contact diameter of the tip as ~16 nm: see the supplementary material for more discussion about the tip contact area. This value is qualitatively in good agreement with previous works, such as $\sim 1.5 \times 10^{-8}$ m^2 K/W for SiO_2-Pt,[4] $\sim 2.0 \times 10^{-8}$ m^2 K/W for Si-Si,[31] and $\sim 2.7 \times 10^{-9}$ m^2 K/W for SiO_2-Au.[27] However, it should be noted that the measured thermal conductance includes heat conduction through solid-solid contact as well as water meniscus and air conduction. Although the contribution of each heat transfer mechanism was not directly measured in the present study, we estimated each thermal conductance using the theoretical model for solid-solid contact,[4] water meniscus,[52] and surrounding air:[1] further discussion can be found in the supplementary material.

The thermal response time of the nanothermometer can also be determined by measuring ΔT_S at different tip scanning speeds. As shown in Fig. 3(c), ΔT_S does not change until the tip scan speed increases to ~1 μm/s, but starts decreasing at higher scan speeds. The inset in Fig. 3(c) compares temperature line profiles as the tip scans across the thermometer sensing area at 0.3 μm/s and 15 μm/s scan speeds, demonstrating that the thermometer cannot fully respond to the tip scan speed at 15 μm/s. The tip scan speed at 1 μm/s is equivalent to the travel time of 7.8 ms between adjacent pixels when a $2\,\mu m \times 2\,\mu m$ area is scanned with a 256×256 resolution. Therefore, the thermal response time that is required for the nanothermometer to reach thermal equilibrium with a moving

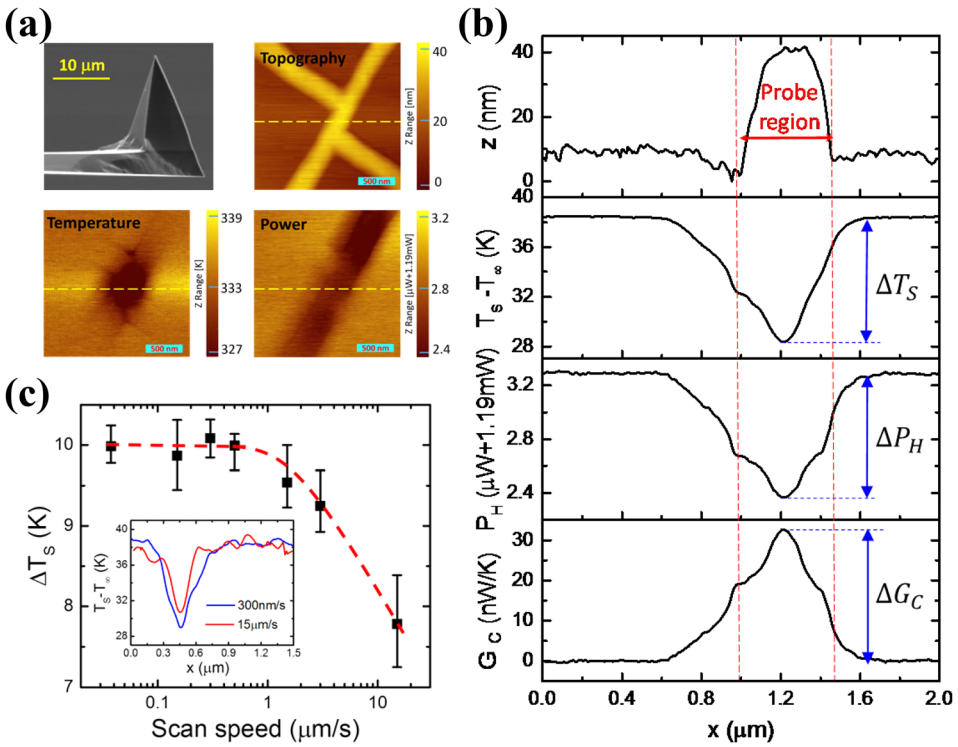

FIG. 3. (a) SEM image of the cantilever tip used as a point heat sink in contact with the nanoheater and the topography image of the thermometer sensing area ($2\,\mu m \times 2\,\mu m$) with its corresponding temperature change and the power dissipation of the Pt nano-strip. (b) The line scan profiles of the topography, thermometer temperature, power dissipation, and the effective thermal conductance when the tip scans along the dashed line in (a). (c) Temperature dip depths of the thermometer sensing area due to tip-induced cooling for different tip scan speeds. The inset compares the temperature line-scan profiles for tip scan speeds at $0.3\,\mu m/s$ and $15\,\mu m/s$. This measurement demonstrates that the nanothermometer cannot fully respond to the tip scan speed higher than $1\,\mu m/s$.

tip can be approximated at ~8 ms. The tip scan speed for all experiments reported in this article was set to $0.3\,\mu m/s$ (~26 ms per pixel) to provide sufficient time for the nanothermometer to thermally respond to the tip-induced cooling.

Fig. 4 shows the *z*-spectroscopy of the cantilever deflection and the corresponding thermometer signal when the cantilever approaches and retracts from the thermometer sensing area. The tip was placed at the thermometer sensing area with feedback-loop control of *x*- and *y*-positions after topographic imaging. The thermometer was joule-heated with the input current of 1.6 mA during the *z*-spectroscopy measurement. The cantilever deflection signal in the top figure depicts the jump-into-contact during the tip approach and the jump-out-of-contact during the tip retraction. The sudden drop and retract points are because of attractive forces between the tip and the substrate due to the capillary and the thermal forces.[27,28,53] The hysteresis of deflection response is due to elastic and possibly plastic deformation of tip and sample, resulting in larger attractive forces during retraction of the tip. The bottom plot also shows temperature jumps in the thermometer signal, corresponding to the contact of the tip. It should be noted that the thermometer z-spectroscopy was obtained by averaging 5 measurements to reduce the noise caused by the z-piezo movement in the AFM. The temperature drop when the cantilever jumps to contact is measured to be 8.3 ± 0.2 K, which is slightly smaller than the temperature dip measured from the scanning experiment (i.e., $\Delta T_S = 10.1 \pm 0.2$ K). We believe that this is because of the slightly off-center position of the tip when the z-spectroscopy was conducted. Nonetheless, the obtained *z*-spectroscopy result confirms that the temperature change of the thermometer is solely due to the local heat transfer from the heated nanothermometer to the cantilever probe upon the contact of the tip.

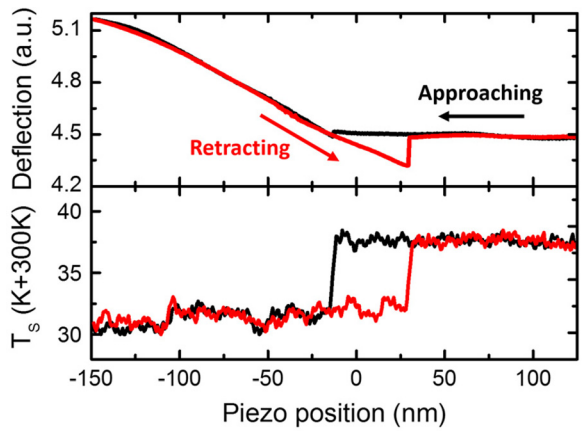

FIG. 4. Z-spectroscopy of the cantilever deflection and the thermometer signal, initially heated at 338.5 K. As the cantilever approaches the thermometer sensing area, the tip jumps into contact on the thermometer to cause a sudden temperature drop. A sudden temperature jump is also observed in the cantilever retraction curve, demonstrating that the thermometer signal change is solely due to local heat transfer through the tip-substrate contact.

In conclusion, on-substrate resistive Pt nanothermometer/nanoheater devices with the sensing area of 250 nm × 350 nm have been fabricated by combining e-beam lithography and photolithography. We believe that the fabricated devices are among the smallest resistive thermometers ever made to date. The sensitivity (or TCR) of the nanothermometer is $(7.0 \pm 0.1) \times 10^{-4}\,K^{-1}$, which is approximately five times smaller than that of a commercially available bulk Pt thermometer, and its noise-equivalent temperature resolution is estimated to be 410 mK. In addition, we have demonstrated that the nanothermometer can be used as a nanoheater by joule-heating the device. By scanning over the heated nanothermometer sensing area with a silicon AFM probe, we measured tip-induced local cooling across the nanoscale point contact. The effective contact thermal conductance is estimated to be 32.5 ± 0.8 nW/K. The obtained

results will provide physical insight into local heat transfer and the resultant temperature distribution in various tip-based thermal engineering technologies.

See supplementary material for the detailed fabrication procedure and topography image of nanothermometers, the estimation of the tip-substrate contact area, the theoretical modeling of thermal conductance for contributing tip-substrate heat transfer mechanisms, the noise spectrum analysis of the nanothermometer, and the numerical simulation of temperature distribution across the nanothermometer when joule-heated.

This work was supported by the National Science Foundation (CBET-1403084 and CBET-1605584) and Nano Material Technology Development Program (2015M3A7B7045518) through the National Research Foundation of Korea (NRF). S.H. and K.P. also thank the startup support from the University of Utah. The AFM was built up partly by the Research Instrumentation Fund from the University of Utah.

[1]A. Majumdar, Annu. Rev. Mater. Sci. **29**, 505 (1999).
[2]M. Hinz, O. Marti, B. Gotsmann, M. A. Lantz, and U. Dürig, Appl. Phys. Lett. **92**, 43122 (2008).
[3]U. F. Wischnath, J. Welker, M. Munzel, and A. Kittel, Rev. Sci. Instrum. **79**, 73708 (2008).
[4]K. Kim, W. Jeong, W. Lee, and P. Reddy, ACS Nano **6**, 4248 (2012).
[5]W. P. King, S. Saxena, B. A. Nelson, B. L. Weeks, and R. Pitchimani, Nano Lett. **6**, 2145 (2006).
[6]J. Lee, A. Liao, E. Pop, and W. P. King, Nano Lett. **9**, 1356 (2009).
[7]S. Jesse, M. P. Nikiforov, L. T. Germinario, and S. V. Kalinin, Appl. Phys. Lett. **93**, 73104 (2008).
[8]M. P. Nikiforov, S. Gam, S. Jesse, R. J. Composto, and S. V. Kalinin, Macromolecules **43**, 6724 (2010).
[9]K. J. Kim, K. Park, J. Lee, Z. M. Zhang, and W. P. King, Sens. Actuators, A **136**, 95 (2007).
[10]S. Somnath, E. A. Corbin, and W. P. King, IEEE Sens. J. **11**, 2664 (2011).
[11]B. Lee, S. Somnath, and W. P. King, Nanotechnology **24**, 135501 (2013).
[12]A. Hammiche, L. Bozec, M. Conroy, H. M. Pollock, G. Mills, J. M. R. Weaver, D. M. Price, M. Reading, D. J. Hourston, and M. Song, J. Vac. Sci. Technol. B **18**, 1322 (2000).
[13]M. Reading, D. Grandy, A. Hammiche, L. Bozec, and H. M. Pollock, Vib. Spectrosc. **29**, 257 (2002).
[14]A. C. Jones and M. B. Raschke, Nano Lett. **12**, 1475 (2012).
[15]G. Binnig, M. Despont, U. Drechsler, W. Häberle, M. Lutwyche, P. Vettiger, H. J. Mamin, B. W. Chui, and T. W. Kenny, Appl. Phys. Lett. **74**, 1329 (1999).
[16]W. P. King, T. W. Kenny, K. E. Goodson, G. Cross, M. Despont, U. Dürig, H. Rothuizen, G. K. Binnig, and P. Vettiger, Appl. Phys. Lett. **78**, 1300 (2001).
[17]D.-W. Lee, T. Ono, T. Abe, and M. Esashi, J. Microelectromech. Syst. **11**, 215 (2002).
[18]W. A. Challener, C. Peng, A. V. Itagi, D. Karns, W. Peng, Y. Peng, X. Yang, X. Zhu, N. J. Gokemeijer, Y.-T. Hsia, G. Ju, R. E. Rottmayer, M. A. Seigler, and E. C. Gage, Nat. Photonics **3**, 303 (2009).
[19]P. E. Sheehan, L. J. Whitman, W. P. King, and B. A. Nelson, Appl. Phys. Lett. **85**, 1589 (2004).
[20]M. Yang, P. E. Sheehan, W. P. King, and L. J. Whitman, J. Am. Chem. Soc. **128**, 6774 (2006).
[21]R. Szoszkiewicz, T. Okada, S. C. Jones, T.-D. Li, W. P. King, S. R. Marder, and E. Riedo, Nano Lett. **7**, 1064 (2007).
[22]A. A. Milner, K. Zhang, and Y. Prior, Nano Lett. **8**, 2017 (2008).
[23]O. Fenwick, L. Bozec, D. Credgington, A. Hammiche, G. M. Lazzerini, Y. R. Silberberg, and F. Cacialli, Nat. Nanotechnol. **4**, 664 (2009).
[24]A. W. Knoll, D. Pires, O. Coulembier, P. Dubois, J. L. Hedrick, J. Frommer, and U. Duerig, Adv. Mater. **22**, 3361 (2010).
[25]D. Pires, J. L. Hedrick, A. De Silva, J. Frommer, B. Gotsmann, H. Wolf, M. Despont, U. Duerig, and A. W. Knoll, Science **328**, 732 (2010).
[26]Z. Wei, D. Wang, S. Kim, Y. Hu, M. Yakes, A. Laracuente, Z. Dai, S. Marder, C. Berger, W. King, W. Heer, P. Sheehan, and E. Riedo, Science **328**, 1373 (2010).
[27]L. Shi and A. Majumdar, J. Heat Transfer **124**, 329 (2002).
[28]K. Park, G. L. W. Cross, Z. M. Zhang, and W. P. King, J. Heat Transfer **130**, 102401 (2008).
[29]K. Kim, J. Chung, G. Hwang, O. Kwon, and J. S. Lee, ACS Nano **5**, 8700 (2011).
[30]W. Lee, K. Kim, W. Jeong, L. A. Zotti, F. Pauly, J. C. Cuevas, and P. Reddy, Nature **498**, 209 (2013).
[31]M. T. Pettes and L. Shi, J. Heat Transfer **136**, 32401 (2013).
[32]K. E. Goodson and M. Ashegh, Microscale Thermophys. Eng. **1**, 225 (1997).
[33]B. McCarthy, Y. Zhao, R. Grover, and D. Sarid, Appl. Phys. Lett. **86**, 111914 (2005).
[34]A. A. Milner, K. Zhang, V. Garmider, and Y. Prior, Appl. Phys. A **99**, 1 (2010).
[35]Y. Yue, X. Chen, and X. Wang, ACS Nano **5**, 4466 (2011).
[36]B. Samson, L. Aigouy, P. Loüw, C. Bergaud, B. J. Kim, and M. Mortier, Appl. Phys. Lett. **92**, 23101 (2008).
[37]K. Kim, J. Chung, J. Won, O. Kwon, J. S. Lee, S. H. Park, and Y. K. Choi, Appl. Phys. Lett. **93**, 203115 (2008).
[38]S. Sadat, A. Tan, Y. Chua, and P. Reddy, Nano Lett. **10**, 2613 (2010).
[39]P. C. Fletcher, B. Lee, and W. P. King, Nanotechnology **23**, 035401 (2011).
[40]E. A. Corbin, K. Park, and W. P. King, Appl. Phys. Lett. **94**, 243503 (2009).
[41]B. Lee and W. P. King, Rev. Sci. Instrum. **83**, 74902 (2012).
[42]D. Chu, D. Bilir, R. Pease, and K. Goodson, J. Vac. Sci. Technol. B **20**, 3044 (2002).
[43]H. Liu, W. Sun, and S. Xu, Adv. Mater. **24**, 3275 (2012).
[44]X. Huo, H. Liu, Y. Liang, M. Fu, W. Sun, Q. Chen, and S. Xu, Small **10**, 3869 (2014).
[45]F. Menges, H. Riel, A. Stemmer, and B. Gotsmann, Nano Lett. **12**, 596 (2012).
[46]S. Sadat, E. Meyhofer, and P. Reddy, Rev. Sci. Instrum. **83**, 84902 (2012).
[47]S. Sadat, E. Meyhofer, and P. Reddy, Appl. Phys. Lett. **102**, 163110 (2013).
[48]D. G. Cahill, Rev. Sci. Instrum. **61**, 802 (1990).
[49]L. Lu, W. Yi, and D. L. Zhang, Rev. Sci. Instrum. **72**, 2996 (2001).
[50]C. Dames and G. Chen, Rev. Sci. Instrum. **76**, 124902 (2005).
[51]X. Zhang, H. Xie, M. Fujii, H. Ago, K. Takahashi, T. Ikuta, H. Abe, and T. Shimizu, Appl. Phys. Lett. **86**, 171912 (2005).
[52]A. Assy and S. Gomès, Nanotechnology **26**, 355401 (2015).
[53]B. Gotsmann and U. Dürig, Appl. Phys. Lett. **87**, 194102 (2005).